ACES Asian Chemical Editorial Society

DOI: 10.1002/cnma.202000058

CHEMNANOMAT
Full Paper

Toward Luminescent Composites by Phase Transfer of $SrF_2:Eu^{3+}$ Nanoparticles Capped with Hydrophobic Antenna Ligands

Thoralf Krahl,*[a, b] Fabian Beer,[a] Alexander Relling,[a] Kornelia Gawlitza,[c] Knut Rurack,[c] and Erhard Kemnitz[a, b]

Abstract: Transparent dispersions of hydrophobic $SrF_2:Eu^{3+}$ nanoparticles in cyclohexane with up to 20% europium were obtained by fluorolytic sol-gel synthesis followed by phase transfer into cyclohexane through capping with SODIUM DODECYLBENZENESULFONATE (SDBS). The particles were characterized by TEM, XRD and DLS as spherical objects with a diameter between 6 and 11 nm in dry state. ^{1}H-^{13}CP MAS NMR experiments revealed the binding of the anionic sulfonate head group to the particle surface. The particles show bright red luminescence upon excitation of the aromatic capping agents, acting as antennas for an energy transfer from the BENZENESULFONATE UNIT to the Eu^{3+} centers in the particles. This synthesis method overcomes the current obstacle of the fluorolytic sol-gel synthesis that transparent dispersions can be obtained directly only in hydrophilic solvents. To demonstrate the potential of such hydrophobized alkaline-earth fluoride particles, transparent luminescent organic-inorganic composites with 10% $SrF_2:Eu^{3+}$ embedded into polyTEGDMA, polyBMA, polyBDDMA and polyD3MA, respectively, were prepared, endowing the polymers with the luminescence features of the nanoparticles.

1. Introduction

Luminescent nanoparticles are of paramount interest for applications ranging from light-emitting devices via information coding to imaging and diagnostics. Among such luminophores, rare-earth doped metal fluorides are a very promising subclass.[1] Besides the classic single-center luminescence, such systems can be tuned in a facile manner to exhibit energy transfer processes, resulting in photon upconversion.[2] A suitable material for such purposes is rare-earth-containing strontium fluoride SrF_2.[3] Photoluminescence quantum yields (PLQYs) are commonly higher than in calcium fluoride CaF_2 because of the lower phonon energy ($SrF_2 = 366\ cm^{-1}$, $CaF_2 = 466\ cm^{-1}$).[4] Moreover, in contrast to the even stronger luminescent BaF_2-based compounds, SrF_2 is still regarded as non-toxic. All these three compounds crystallize in the cubic fluorite structure, which can be described as cubic closest packing of cations (Ca^{2+}, Sr^{2+} or Ba^{2+}) with anions (F^-) occupying tetrahedral cavities. Strontium fluoride SrF_2 is able to form solid solutions with up to 45% of rare-earth fluorides LnF_3 (Ln = Y, La…Lu) while retaining its cubic crystal structure.[5] These phases have a sum formula of $Sr_{1-x}Ln_xF_{2+x}$ ($x = 0 - \approx 0.45$). The structure of the corresponding $Ca_{1-x}Ln_xF_{2+x}$ has been thoroughly investigated.[6] Sr compounds were less intensively studied, but the structural features were largely similar.[7] In general, Ca^{2+}/Sr^{2+} and Ln^{3+} share a common regular lattice site of the cubic fluorite structure. Regular fluoride ions occupy tetrahedral cavities; surplus fluoride ions occupy octahedral cavities. For medium rare-earth contents ($x > 0.01$), the fluoride ions form anionic clusters in the structure, while the cation sublattice remains intact. A thorough discussion of the structural features can be found elsewhere.[6–7]

For unperturbed and efficient luminescence, a purely statistic distribution of the cations Sr^{2+} and Ln^{3+} is desired instead of the formation of Sr-rich and Ln-rich domains. In reality, the distribution of the metal ions is determined by the synthesis method. An overview can be found in ref.[1a] The most common methods are thermal decomposition (mostly of trifluoroacetates), solvothermal synthesis or precipitation from aqueous solution. Often hydrophobic nanoparticles are obtained, which can be transferred into hydrophilic particles in a second step by oxidative cleavage of the double bond of the capping agent oleic acid. However, most of these synthesis methods lack the capability of a proper upscaling, and hence, only small amounts of a few grams can usually be synthesized.

Hydrophilic nanoparticles at the few hundred grams up to the kilogram scale can yet be synthesized in a straightforward manner directly at room temperature without any further purification step using the fluorolytic sol-gel synthesis.[8] Transparent sols of rare-earth containing SrF_2 nanoparticles are obtained by reacting alkaline earth lactate and rare-earth

[a] Dr. T. Krahl, MSc. F. Beer, B.Sc. A. Relling, Prof. Dr. E. Kemnitz
Institut für Chemie
Humboldt-Universität zu Berlin
Brook-Taylor-Str. 2, D-12489 Berlin (Germany)
E-mail: thoralf.krahl@chemie.hu-berlin.de

[b] Dr. T. Krahl, Prof. Dr. E. Kemnitz
Nanofluor GmbH
Rudower Chaussee 29, D-12489 Berlin (Germany)
E-mail: th.krahl@nanofluor.de

[c] Dr. K. Gawlitza, Dr. K. Rurack
Fachbereich Chemische und optische Sensorik
Bundesanstalt für Materialforschung und –prüfung (BAM)
Richard-Willstätter-Str. 11, D-12489 Berlin (Germany)

Supporting information for this article is available on the WWW under https://doi.org/10.1002/cnma.202000058

acetate dissolved in ethylene glycol with anhydrous methanolic hydrogen fluoride.[3] Lactic and acetic acid formed during the synthesis stabilize the particles' surface. These particles show extraordinary luminescence properties because for cubic *nano*-$Sr_{0.6}Eu_{0.4}F_{2.4}$ (= SrF_2:Eu40) and *nano*-$Sr_{0.7}Tb_{0.3}F_{2.3}$ (= SrF_2:Tb30) cross relaxation is still extremely low, which is quite unusual for such compounds. Commonly, the luminescence intensity decreases for rare-earth contents above 20%.[9] These nanoparticles can be incorporated into PMMA (poly(methyl methacrylate)) to obtain transparent composites with tunable luminescence.[3b] By incorporating both Eu-containing and Tb-containing particles simultaneously, red or green luminescence of such composites can be achieved by tuning the excitation wavelength. Incorporation of *nano*-$Sr_{0.88}Yb_{0.10}Er_{0.02}F_{2.12}$ (= SrF_2:Yb10,Er2) leads to composites capable of photon upconversion, i.e. transforming IR radiation into visible light.

In general, obtaining a transparent dispersion of these nanoparticles in an organic polymer is challenging. Dispersion in a hydrophilic thermoplastic polyester such as polylactic acid (PLA) worked well.[10] In addition, as mentioned above, methyl methacrylate and its polymer PMMA also disperse the nanoparticles to a certain extent. However, this method is limited to a few acrylate systems only. As a rule, particles from the fluorolytic sol-gel synthesis are always hydrophilic and cannot be dispersed directly in a more hydrophobic acrylate monomer like e.g. D3MA (1,10-decandiol dimethacrylate). Thus, either further functionalization of the particle surface is necessary[11] or the composition of the acrylate system must be adjusted by addition of a certain amount of hydrophilic comonomers such as HEMA (2-hydroxyethyl methacrylate) and BisGMA (bisphenol A-glycidyl methacrylate).[12] See SI Figure S1 for formulas of all acrylates used in this work.

The aim of the work presented here was to explore the possibility of adapting the particles to the polymer instead of vice versa. Although PMMA is a widely used polymer, its applications are limited due to its comparatively low thermal stability and low hardness. Dimethacrylates like D3MA or TEGDMA (triethylene glycol dimethacrylate) are ingredients of many monomer resins, which result in harder polymers than PMMA. However, those resins containing hydrophobic dimethacrylates are not compatible with particles capped with lactic acid.

An approach to hydrophobic nanoparticles directly from the fluorolytic sol-gel synthesis should thus avoid the liberation of lactic or other carboxylic acids from the metal precursor salts during synthesis, which strongly bind to the particle surface and form a hydrophilic outer layer. Although the solubility of the precursors is not a premise to obtain water-clear transparent sols, in the case of luminescent solid solutions soluble precursors other than lactates and acetates are required to ensure the best possible statistic distribution of the cations inside the nanoparticles. This leaves only a limited amount of suitably soluble strontium precursors. Strontium alkoxides would in general be appropriate, but most of them are highly susceptible to oxidation and must be treated under inert gas. A more practicable precursor is $Sr(OH)_2 \cdot 8H_2O$. This compound is soluble in ethylene glycol, while $Ca(OH)_2$ and $Ba(OH)_2 \cdot 8H_2O$ are not. The only byproduct formed during fluorination is water, which can be easily removed. A corresponding europium source for this kind of synthesis is the soluble $Eu(NO_3)_3 \cdot 6H_2O$ salt. Europium chloride is unsuitable for that purpose, because the formation of the thermodynamically more stable SrClF is favored over the formation of SrF_2.[13]

The present work introduces an elegant synthesis route to highly luminescent hydrophobic SrF_2:Eu^{3+} nanoparticles, which can be easily upscaled. The primary synthesis in ethylene glycol is followed by extraction into cyclohexane using SDBS (sodium dodecylbenzenesulfonate) as phase transfer reagent. The obtained hydrophobic nanoparticles were thoroughly characterized, and their potential for producing luminescent organic-inorganic composites was investigated.

2. Results and Discussion

2.1. Synthesis

Using $Sr(OH)_2 \cdot 8H_2O$ and $Eu(NO_3)_3 \cdot 6H_2O$ as reactants for the fluorolytic sol-gel synthesis, the equation for the stoichiometric fluorination can be written as follows (x = 0–0.2):

$$(1\text{-}x)\ Sr(OH)_2 \cdot 8H_2O + x\ Eu(NO_3)_3 \cdot 6H_2O + (2+x)\ HF_{aq} \rightarrow Sr_{1-x}Eu_xF_{2+x} + 3x\ HNO_3 + (10\text{-}4x)\ H_2O \quad (1)$$

In reality, 0.05 eq HF less than shown in eq. 1 were used for the fluorination. This leaves a small number of unreacted sites at the particle surface, thus offering the possibility for subsequent functionalization. The synthesis is straightforward for $x \geq 0.05$, i.e. when the rare-earth content is at least 5%. A small amount of HNO_3 is formed during the synthesis upon consumption of the europium nitrate (0.6 eq in the case of SrF_2:Eu20), the strong acid protonating non-reacted surface OH groups thus preventing particle agglomeration. In the case of SrF_2 and SrF_2:Eu1, in which either no or only small amounts of HNO_3 are formed (0.03 eq in the case of SrF_2:Eu1), the particles remain agglomerated while stirring. Here, a slight excess of HNO_3 is added, leading to deagglomeration of the nanoparticles and the formation of a clear sol (see Table 5). Pure SrF_2 and samples with 1%, 5%, 10% and 20% Eu^{3+} were synthesized via this method for the spectroscopic studies. One sample with 5% Y^{3+}, which is a diamagnetic ion, was synthesized for solid-state NMR experiments.

After one day of stirring, a transparent, nearly water-clear sol was obtained (Figure 1). The ratio of ethylene glycol/water in the final sol was approx. 80:20 mainly due to the released crystal water of the strontium precursor. The formation of transparent sols was unexpected because the presence of water in the fluorolytic sol-gel synthesis in monohydric alcohols like methanol, ethanol or isopropanol usually prevents transparency through the O(H)-bridges of water inducing particle aggregation. Additionally, Ostwald ripening of the nanoparticles may occur, especially when the amount of water is large. In contrast

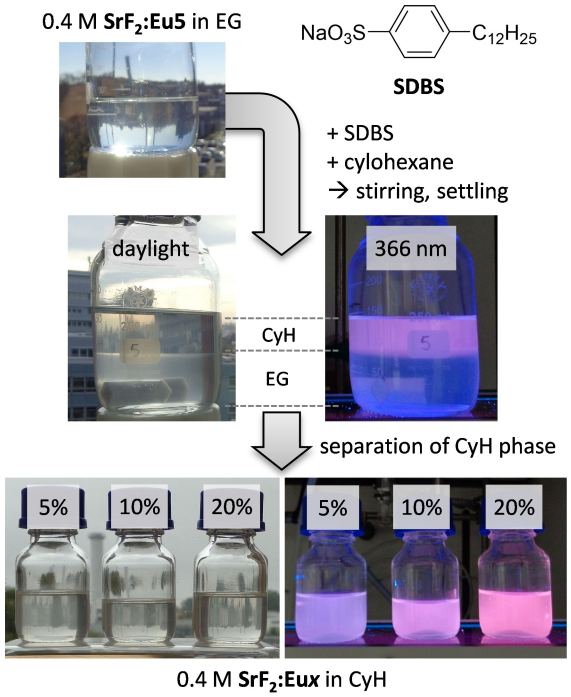

Figure 1. Synthesis overview. EG = ethylene glycol, CyH = cyclohexane. SDBS is a mixture of isomers.

to mono-alcohols, the reactivity of water is greatly reduced in ethylene glycol solution due to solvation by the polyhydric alcohol. Additionally, the reactivity of HF is increased already by small amounts of water due to protolysis. Combination of both effects thus presumably leads to the fast formation of clear sols. Although ethylene glycol supports fast deagglomeration and stabilization of primary nanoparticles, resulting in a clear and transparent dispersion, these sols are not stable on a long-term scale. After two weeks, a white haze begins to develop, which slowly precipitates during the next weeks. This is in contrast to the sols stabilized with lactic acid, which are stable for years.[3] Obviously, agglomeration or Ostwald ripening is not totally suppressed here. Therefore, the extraction should be performed within a couple of days.

Mixing these sols with SDBS and cyclohexane led to white slurry. After allowing settling overnight, a two-phase system was obtained. The upper transparent cyclohexane phase contained the luminescent nanoparticles. This is impressively demonstrated by illumination of the mixture with UV light (Figure 1). The red luminescence of Eu^{3+} is observed in the cyclohexane phase only. The luminescence intensity is approximately the same as previously in the ethylene glycol phase, provided that the volume of both solvents is the same. Careful investigation of the ethylene glycol phase after separation frequently revealed a certain residual red luminescence, the total intensity of which however never exceeded 0.5% of that of the cyclohexane phase (see SI Figure S2). This is strong evidence that virtually all particles have been successfully transferred to the cyclohexane phase. In a control experiment, pure ethylene glycol was mixed with SDBS, cyclohexane and the appropriate amount of water and HNO_3. After phase separation, no SDBS was found in the upper phase. Thus, DBS anions will only migrate to the hydrophobic phase in the presence of nanoparticles.

The cyclohexane phase was separated using a separator funnel for larger amounts or a syringe for smaller amounts. The extraction also worked well for cyclopentane and cycloheptane, but the performance of *n*-alkanes was inferior. *n*-Alkanes could extract particles, but the hydrophobic phase remained whitish and turbid. We ascribe this behavior to the weaker dispersion forces of *n*-alkanes. For comparison, the lower boiling point of *n*-hexane 69 °C vs. cyclohexane 81 °C hints to weaker dispersion forces in *n*-alkanes than in cycloalkanes. We conclude that the dispersion forces between the hydrophobic particle surface and the solvent are weaker in *n*-alkanes than in cycloalkanes. Therefore, the tendency of the particles to agglomerate is higher in *n*-alkanes.

Although the primary synthesis in ethylene glycol was also successful for higher contents of Eu, namely SrF_2:Eu40 (which is a single cubic phase) and even SrF_2:Eu75 (which in reality is a mixture of a Sr-rich phase $Sr_{1-x}Eu_xF_{2+x}$ and an Eu-rich phase $Eu_{1-y}Sr_yF_{3-y}$), unfortunately, extraction of these particles into cyclohexane failed. No phase separation occurred after addition of SDBS and cyclohexane, which seems to be caused by the large amounts of nitric acid formed during the synthesis. Phase separation also failed after neutralization of the HNO_3 by NH_3 or NaOH.

2.2. Characterization of the particles

Thorough characterization was done on particles **1**, **3**, **4** and **5** with 0, 5, 10 and 20% Eu, respectively. Particles **6** with 5% Y were used for solid-state NMR to suppress paramagnetic effects of Eu^{3+}. Particles **2** with 1% Eu were used for luminescence characterization only (see next section).

The sols in cyclohexane are water-clear and transparent, indicating small particle sizes. TEM images show nearly spherical particles with a diameter between 5 and 14 nm (Figure 2 and Table 1). The particle size slightly decreases with increasing Eu content. This seems to be a general trend in solid state chemistry and is consistent with previous results.[3a]

According to DLS measurements, the hydrodynamic diameters are approximately 20 nm (see SI Figure S3). Drying of the sols in vacuum yields white powders. XRD data of these powders show typical reflections of cubic SrF_2 nanoparticles (see SI Figure S4). According to Scherrer's equation, the size of

Table 1. Particle diameter extracted from statistical evaluation of TEM images and size of the coherent scattering region from XRD (see Experimental for details).

	TEM size [nm]	XRD size [nm]
1b/**1c** SrF_2	11 ± 3	13 ± 1
3b/**3c** SrF_2:Eu5	9 ± 2	11 ± 2
4b/**4c** SrF_2:Eu10	8 ± 2	10 ± 2
5b/**5c** SrF_2:Eu20	6 ± 1	9 ± 3

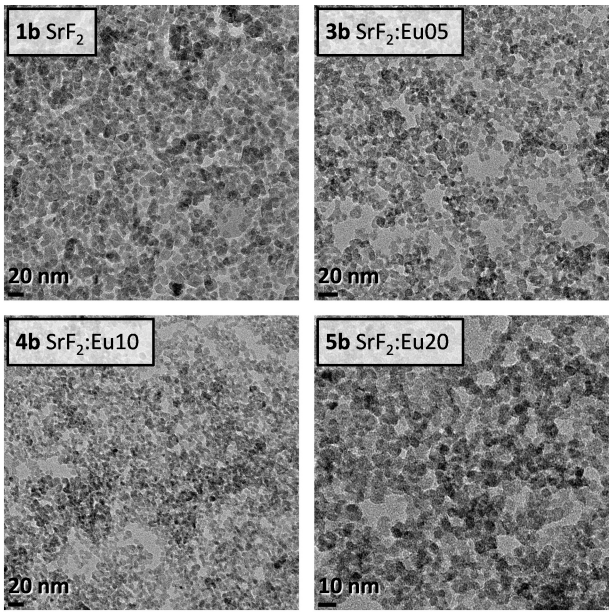

Figure 2. TEM images of SrF_2 and various SrF_2:Eu^{3+} nanoparticles cast from 8 mM cyclohexane dispersions.

the coherent scattering region is similar to the size taken from TEM images (Table 1). The cubic lattice parameter slightly decreases with increasing Eu^{3+} contents (see SI Figure S4), which is consistent with data published previously for single crystals.[5]

For the initial extraction with cyclohexane, 10 mol-% of SDBS (relative to Sr + Ln) was added as phase transfer reagent. Elemental analyses of the final dry SrF_2:Eu^{3+} powders are given in Table 2 together with the measured ignition loss at 500 °C in air. From these data, the molar ratio DBS/SrF_2:Ln*x* was calculated (Table 2). For the rare-earth-free **1c** SrF_2, this ratio is only 6.5%, which is lower than expected. For the rare-earth-containing powders, the amounts of organics and hence of DBS anions, are higher and close to the expected 10%.

Detection of sodium in the powders by EDX analysis was not possible, leading to the conclusion that the dodecylbenzylsulfonate anions are electrostatically bound to native protonated sites on the particle surface, facilitating phase transfer, while the sodium ions remain in the hydrophilic phase. As additional information, thermal analysis of one powder is given in SI Figure S5.

To identify the exact nature of the organic species adsorbed at the particle surface, ^{1}H-^{13}C CP MAS NMR spectra of diamagnetic **6c** SrF_2:Y5 powder were recorded (Figure 3). Y^{3+} is a diamagnetic ion used here instead of paramagnetic Eu^{3+} that usually interferes with NMR measurements. Pure SDBS shows several signals between 10 and 50 ppm of the aliphatic side chain, and three signals between 125 and 150 ppm for the aromatic ring (see experimental section for details). The spectrum of **6c** SrF_2:Y5 shows the same signals and an additional signal at 63.2 ppm. The latter signal is due to ethylene glycol. Obviously, not only the particles are extracted into the hydrophobic phase, but also a small amount of the primary solvent. The amount of ethylene glycol cannot be quantitatively estimated from the CP NMR experiments. Calculation of the hypothetical ignition loss due to DBS is very close to the measured ignition loss (Table 2). Thus, the amount of ethylene glycol is obviously small compared to the actual surfactant.

As already mentioned in the previous section, in a control experiment no ethylene glycol and DBS anions were extracted into cyclohexane without particles. This leads to the conclusion that a small portion of ethylene glycol is still bound to the particles' surface together with the DBS anions. No pronounced signal of adsorbed cyclohexane (expected at ≈27 ppm)[14] was observed, yet small amounts would not be detectable due to coverage by the intense signal of the CH_2 units of the side chain. If adsorbed cyclohexane is still present in the powder, its amount is below the detection limit.

2.3. Luminescence properties

All sols containing Eu^{3+} show red luminescence upon excitation with UV light. Luminescence emission spectra of direct excitation of Eu^{3+} at 393 nm are shown in Figure 4a. Three main strong and narrow emission bands due to $^5D_0 \rightarrow {}^7F_J$ transitions are observed: 590 nm ($J=1$), 610 nm ($J=2$) and 698 nm ($J=4$). The transitions at 580 nm ($J=0$) and 650 nm ($J=3$) are forbidden by selection rules and significantly weaker, the $^5D_0 \rightarrow {}^7F_0$ transition is only expressed as a small shoulder. This is the typical spectrum of Eu^{3+} ions observed for doped nanoparticles.[3a,9a,b,15] The emission lines do not show significant splitting. In nanoparticles, each Eu^{3+} center has a slightly different surrounding. The difference between Eu^{3+} in the particle center and Eu^{3+} near the particles surface is most prominent. The resulting emission spectrum is a superposition of the emission of all centers, and hence, all influences from crystal field splitting are averaged out.

Table 2. Comparison of elemental analysis (C, H, S, N) and ignition loss. No sodium was detected in EDX analysis. See experimental section for calculation details.

	measured data					calculated data	
Sample	C [%]	H [%]	S [%]	N [%]	ignition loss [%]	molar ratio DBS:metal [%]	ignition loss from DBS only [%]
1c SrF_2	8.35	1.35	1.37	0.215	13.1	≈6.4	13.9
3c SrF_2:Eu5	10.99	1.71	1.68	0.165	16.8	≈8.2	17.1
4c SrF_2:Eu10	11.50	1.82	1.86	0.187	17.2	≈9.5	18.9
5c SrF_2:Eu20	11.19	1.79	1.77	0.236	17.7	≈9.5	18.0
6c SrF_2:Y5	11.97	1.85	1.90	<0.1	18.2	≈9.2	19.3

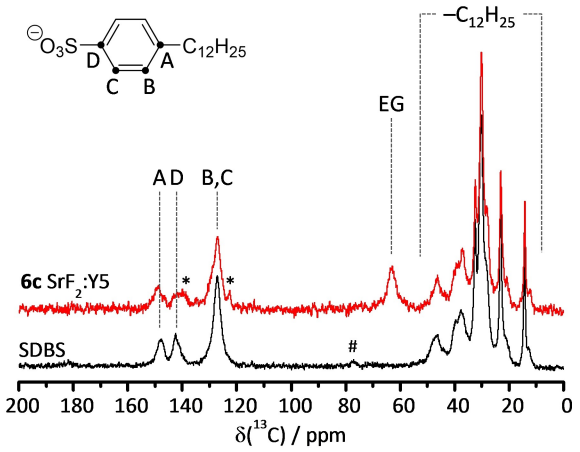

Figure 3. ^{1}H-^{13}C CP MAS NMR spectra of neat SDBS and **6c** SrF_2:Y5 powder. EG: ethylene glycol, *: spinning side band, #: unknown impurity. The $C_{12}H_{25}$ chain is a mixture of isomers.

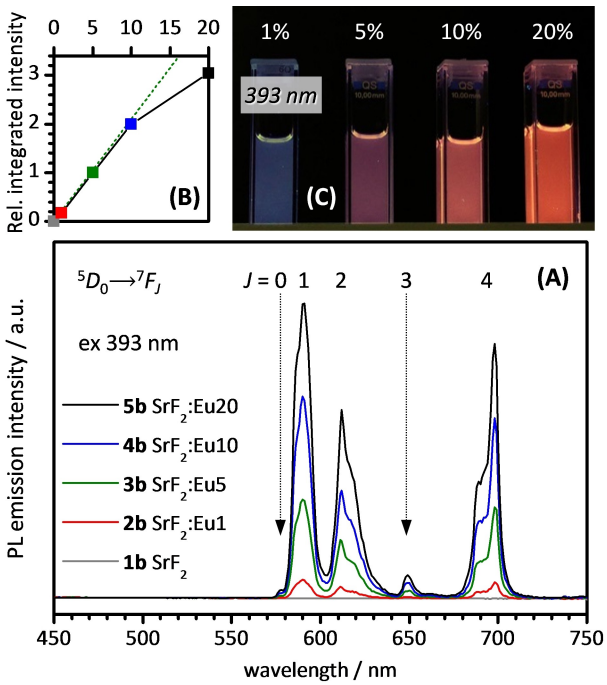

Figure 4. A: Photoluminescence emission spectra of 0.4 M SrF_2:Eu^{3+} in cyclohexane, direct excitation of Eu^{3+} at 393 nm. B: Integrated emission intensity relative to SrF_2:Eu5. C: Sols illuminated at 393 nm.

The total integrated emission intensity increases linearly up to 10% Eu^{3+} due to higher concentration of emission centers in the sol, while the total metal concentration remains constant. At still higher concentration (20% Eu^{3+}), the intensity still increases but deviates from linearity (Figure 4b), i.e. **5b** with 20% Eu^{3+} has less than twice the intensity as compared to **4b** with 10% Eu^{3+}.

Luminescence quantum yields decrease from 29.2% for 1% Eu^{3+} to 19.5% for 20% Eu^{3+} when excited in the near UV region (Table 3). Similar trends have been reported before for Eu^{3+} doped at various levels into host lattices that do not absorb in the UV/vis such as $ZnAlO_4$, with absolute PLQYs in a range of 18–32% that is comparable to the values found here.[16] The decrease of the PLQYs correlates well with a decrease of the mean lifetime of the excited state of Eu^{3+} from 3.78 ms for Eu^{3+} to 2.27 ms for 20% Eu^{3+} (Table 3, see SI Figure S6 for decay curves). A similar trend as a function of dopant concentration has, for instance, also been reported for Eu^{3+}-doped $ZnAlO_4$ (with 0.05–5% Eu^{3+}), and average lifetimes between 1 and 4 ms were also found for similar systems with capping ligands.[3a,9a,b,16] Core-shell particles or microcrystals usually exhibit longer lifetimes.[3b,17]

The decrease of PLQY and luminescence lifetime and the deviation of the emission intensity from linearity are caused by increasing non-radiative cross relaxation of neighboring Eu^{3+} centers. However, the influence of this mechanism of non-radiative relaxation is still comparatively small, i.e., only a factor of approx. 1.6 in emissivity compared to a factor of 20 in concentration.

It is noteworthy to mention that the luminescence decay cannot be fitted using a single exponential function. This is the typical behavior of nanoparticles.[18] Luminescence centers in the middle of the particle have a longer lifetime than those near the surface. Consequently, only a mean lifetime $\bar{\tau}$ can be given (see experimental section for details).

Surprisingly, excitation of the sols with short wave UV light below 300 nm results in a very intense red luminescence. The corresponding emission spectra are given in Figure 5a. This is somehow unexpected, because excitation of Eu^{3+} in this wavelength region is not very efficient. The same emission bands are observed as described above with different intensity ratios of the single transitions, additionally varying between the samples. Despite the differences in the intensity ratios, the total integrated emission intensity upon excitation below 300 nm is virtually constant for 5–20% Eu^{3+} and drops only for 1% Eu^{3+} (Figure 5b).

Table 3. Luminescence properties of SrF_2:Eu^{3+} in cyclohexane. $\bar{\tau}$: mean luminescence lifetime, I_{rel}: emission intensity relative to SrF_2:Eu5, R: asymmetry ratio $I_{em}(^5D_0 \rightarrow {}^7F_2)/I_{em}(^5D_0 \rightarrow {}^7F_1)$, Φ_{PL}: photoluminescence quantum yield.

Sample	ex 393 nm				ex 278 nm			
	$\bar{\tau}$ [ms]	I_{rel}	R	Φ_{PL}	$\bar{\tau}$ [ms]	I_{rel}	R	Φ_{PL}
2b SrF_2:Eu1	3.78	0.18	0.78	29.2%	2.38	0.14	1.26	1.3%
3b SrF_2:Eu5	3.31	1	0.78	26.8%	2.39	1	1.17	6.4%
4b SrF_2:Eu10	3.13	2.00	0.71	24.9%	2.50	0.91	0.95	6.0%
5b SrF_2:Eu20	2.27	3.04	0.73	19.5%	2.10	1.11	0.79	6.8%

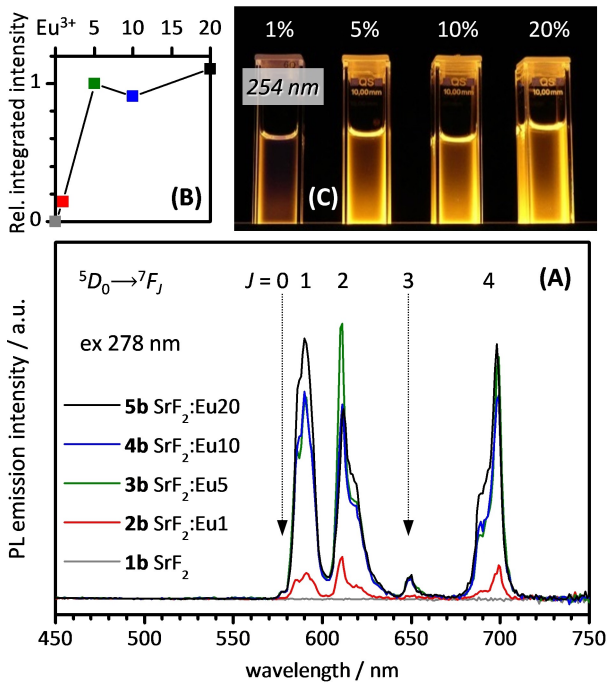

Figure 5. A: Photoluminescence spectra of 0.4 M SrF_2:Eu^{3+} in cyclohexane, excitation of aromatic system at 278 nm. B: Integrated emission intensity relative to SrF_2:Eu5.C: Illumination of the sols at 254 nm.

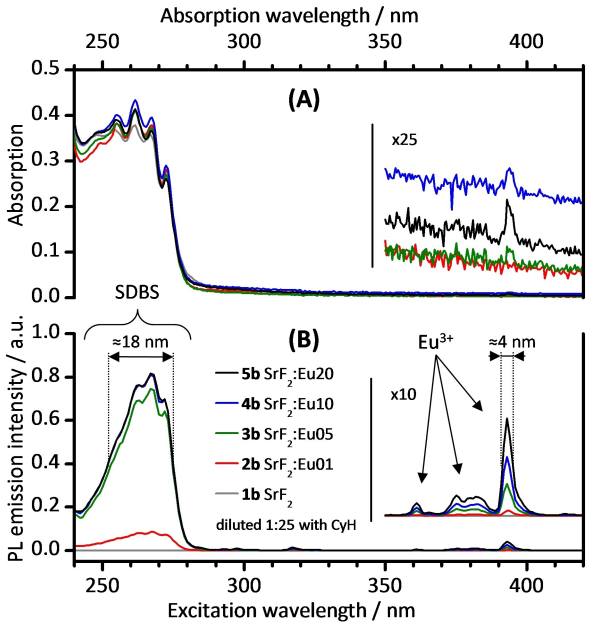

Figure 6. Comparison of (A) absorption spectra and (B) luminescence excitation spectra (λ_{em} = 590 nm) of 16 mM SrF_2:Eu^{3+} in CyH. FWHM values of important bands are given. The absorption spectra of 1b SrF_2 and 2b SrF_2:Eu01 are virtually overlapping in the area > 300 nm.

Thus, another mechanism seems to be responsible for the intense UV-excited emission. The aromatic system of the alkylbenzenesulfonate anion is easily excited at < 280 nm.[19] Because of the considerably small size of the particles and when the particles are doped with a sufficient amount of Eu^{3+}, sensitization of luminescent rare-earth centers in the particles can occur. To prove this assumption, absorption and excitation spectra are compared in Figure 6. The absorption spectra of the particles in cyclohexane show the strong absorption band of the DBS anion between 240 and 280 nm. The absorption of Eu^{3+} can be additionally seen as a tiny peak at 393 nm (see inset). The excitation spectra show the same strong band between 240 and 280 nm as the absorption spectra, indicative of energy transfer from DBS to Eu^{3+}. This assumption is supported by measurements of PLQYs and luminescence lifetimes (Table 3). Excitation of the aromatic moiety leads to Eu^{3+} PLQYs of only ≈6% for 5–20% Eu^{3+} (no variation with Eu^{3+} content) compared to PLQY of 20 to 30% for direct excitation of Eu^{3+}. Quantum yields of 20 to 30% are also observed for Eu^{3+} doped alkaline earth fluoride nanoparticles in protic solvents.[3a] For core-shell particles, the quantum yields increase to more than 50% due to reduced surface relaxation.[3b] Energy transfer from DBS to Eu^{3+} leads to a certain reduction in the mean luminescence lifetime of Eu^{3+} compared to direct excitation.

The sensitization pathway can also be rationalized in terms of other Eu^{3+}-doped metal fluoride and metal oxide nanoparticles published previously in the literature. For instance, when Eu^{3+} ions are doped into nanoparticles composed of metal oxide host lattices, broad and unstructured bands in the 200–300 nm region of the excitation spectra can commonly be found, which however can differ largely in intensity depending on the type of host matrix. When no other UV-absorbing auxochrome is present in the host such as, e.g. in $ZnAl_2O_4$ or $Y_2Sn_2O_7$, the intensity of this broad band is commonly rather low and very similar to that of the Eu^{3+}-centered transitions, because it arises from charge transfer-type $O^{2-}\rightarrow Eu^{3+}$ transitions.[16,20] However, when other auxochromes are present, like in $La_2Hf_2O_7$ or YVO_4, the bands in that region of the excitation spectrum are commonly much more intense than the Eu^{3+}-centered excitation bands, because they stem from one of the building blocks of the host lattice (e.g., hafniate or vanadate) and sensitize the Eu^{3+} luminescence via energy transfer, in the same way as the organic entities are operating in our system.[21] In case of metal fluoride host matrices, neither auxochromic nor $O^{2-}\rightarrow Eu^{3+}$ type bands can commonly be observed in the luminescence excitation. Only when for instance the doping level of Eu^{3+} is considerably high so that a significant amount of Eu^{3+} centers can lie at the surface and interact with their environment putatively offering oxygen atoms, such bands start to be observable.[9b]

Interestingly, the asymmetry ratio $R = I_{em}(^5D_0\rightarrow{}^7F_2)/I_{em}(^5D_0\rightarrow{}^7F_1)$, which is the ratio between the integrated emission intensity at 615 and 590 nm, changes upon excitation of the aromatic system (Table 3). For 1% and 5% Eu^{3+}, the hypersensitive electric $J=2$ emission is more intense than the magnetic $J=1$ transition ($R>1$). For 20% the opposite is true ($R<1$), and for 10% both are of nearly equal intensity (Figure 5a). This effect is not observed for the direct excitation of Eu^{3+}, where R remains nearly constant ≈0.75.

The $J=2$ emission is only allowed for those Eu^{3+} having no inversion symmetry. The energy transferred from the aromatic capping agent to the particle is not transferred into the whole particle, but selectively excites Eu^{3+} centers near the particle surface. These Eu^{3+} sites have a lower symmetry than those deeper inside the particle, and hence, the $J=2$ transition is increased relative to $J=1$. While the average site symmetry of the whole particle seems to be independent of the Eu content, the surface site symmetry increases from 1 to 20% Eu^{3+}.

Apparently, the DBS anions are adsorbed via the sulfonate group at the particle surface, allowing the particles to form a colloidal dispersion (=sol) in cyclohexane. The high luminescence intensity in the red visible range upon short-wave UV excitation (250–280 nm) is caused by the distinctly higher molar absorption coefficient of the DBS anion compared with Eu^{3+}. DBS itself is only weakly fluorescent in the near-UV range (see SI Figure S7).[19a] Energy transfer from the aromatic moiety occurs mainly to Eu^{3+} in close spatial proximity to the DBS anions, i.e., to those Eu^{3+} ions located close to the surface. Because on the millisecond time scale, excited surface-near Eu^{3+} centers are usually susceptible to interaction with solvent molecules, they often show higher non-radiative relaxation and reduced luminescence. A comparison of the data between UV- and direct Eu^{3+} excitation reflects these effects well.

When the capping ligand is excited, the overall emission intensity for 5–20% Eu^{3+} is primarily determined by the amount of energy absorbed by the DBS anions, and not by the amount of Eu^{3+}. If sufficient Eu^{3+} centers are present within a single-digit nanometer distance from the aromatic antenna, the amount of energy transferred from DBS anions to Eu^{3+}, and thus PLQYs and lifetimes, will remain virtually constant. Only at Eu^{3+} contents as low as 1%, energy transfer efficiency is reduced because of a limited local acceptor concentration, resulting in PLQYs below 2%.

For 16 mM SrF_2:Eu5, the red Eu^{3+} emission intensity is increased by a factor of ≈110 (see SI Figure S8) upon excitation of the DBS ligand at 267 nm compared to the direct excitation of Eu^{3+} at 393 nm. When polychromatic light is used for excitation, the enhancement factor may be different due to different widths of the absorption bands (Figure 6).

The opposite trends in the luminescence quantum yields upon near-UV and mid-UV excitation as evident from Table 3 are also in line with literature reports. While the decrease in PLQY with increasing Eu^{3+} doping level has also been mentioned above, host-sensitized systems such as YVO_4:Eu^{3+} with Eu^{3+} doping from 1–40 at-% show an increase in PLQY until 10% doping level and a constant value thereafter.[22] As would be expected, with the sensitizer being even closer located to the emitters than in our system, absolute PLQYs are higher, e.g. from 5% for 2% Eu^{3+} via 7% for 5% Eu^{3+} to 15% for 10–40% Eu^{3+}.[23] Also, such systems show a biexponential decay behavior.

3. Composites

In a first step toward actual application of such nanoparticles in luminescent materials, we approached the synthesis of organic-inorganic polyacrylate composites using the hydrophobic nanoparticles. An essential requirement on such composites is optical transparency. A larger batch (500 mL) of **3b** SrF_2:Eu5 (0.4 M sol in cyclohexane) was used for these experiments. In a first attempt, the sol was spray-dried, resulting in a very fine white powder. Unfortunately, re-dispergation of this powder in organic solvents or acrylate monomers was unsuccessful even when using a high energy sonotrode. Obviously, the nanoparticles aggregate irreversibly during the drying process.

Therefore, another method was developed. The sols in cyclohexane were mixed with acrylate monomers, followed by evaporation of the solvent in vacuum. Applying this procedure, the particles always formed stable dispersions, greatly reducing potential self-aggregation. Evaporation of cyclohexane (b.p. 81 °C) is straightforward except in the case of MMA (methyl methacrylate, b.p. 101 °C). For the latter monomer, sols in cyclopentane (b.p. 49 °C) were employed. All other acrylates possess boiling points of 250 °C and higher. The volume ratio of acrylate/sol was 1:2, resulting in an approx. 10% dispersion of SrF_2:Eu5 in the monomer. After addition of the photo-initiator, the dispersion was polymerized under UV light. Results are summarized in Table 4, see SI Figure S1 for chemical formulas of the acrylates.

The hydrophilic monomer HEMA and the fluorous monomer OMA-F13 (tridecafluorooctyl methacrylate) already became turbid upon mixing with the sol. This is not surprising, because neither of them is really compatible with cyclohexane and a hydrophobic particle surface bearing C12 units.

MMA is somewhat ambivalent. Upon mixing with the sol, a clear dispersion remained, yet after evaporation of the solvent, it became turbid and stayed like that upon polymerization. Thus, MMA and PMMA are still not hydrophobic enough to host these types of particles. Admixture of 20% LMA (linear C12 methacrylate) to 80% MMA was then invoked to use a more hydrophobic mixture than pure MMA. The idea was to increase interaction of the long chains of LMA with the C12 side chains

Table 4. Synthesis of organic-inorganic composites. Inorganic mass content of composites is ≈10%.

Monomer		Monomer + 0.4 M SrF_2:Eu5 in CyH (1:2)		
Name	*logP*[a]	*After mixing*	*After evaporation*	*After polymerization*
HEMA	0.47	turbid	turbid	turbid
MMA[b]	1.38	clear	turbid	turbid
TEGDMA	1.88	clear	clear	clear[c]
BMA	2.88	clear	clear	clear[c]
BDDMA	≈3.2	clear	clear	clear[c]
D3MA	≈5.5	clear	clear	clear[c]
OMA-F13	≈5.9	turbid	turbid	turbid

[a] Logarithm of partition coefficient octanol/water (CyH 3.44; EG −1.36).[24] [b] Cyclopentane as solvent for SrF_2:Eu5. [c] See Figure 7; MMA = methyl methacrylate, HEMA = 2-hydroxyethyl methacrylate, BMA = butyl methacrylate, BDDMA = 1,4-butandiol dimethacrylate, TEGDMA = triethylene glycol dimethacrylate, D3MA = 1,10-decandiol dimethacrylate, OMA-F13 = tridecafluorooctyl methacrylate.

of the DBS anions on the particles' surface. Unfortunately, the dispersion of the particles in this monomer mixture also became turbid during evaporation.

Finally, the more hydrophobic TEGDMA, BMA (butyl methacrylate), BDDMA (1,4-butanediol dimethacrylate), and D3MA all performed successfully. In these cases, clear dispersions of nanoparticles in the monomer were obtained. Out of these dispersions, transparent composite slabs were polymerized (Figure 7). Upon UV excitation, these slabs exhibit the red luminescence of Eu^{3+} (see SI Figure S9 for spectra and SI Table S1 for lifetimes). All slabs show the typical spectra of Eu^{3+} accompanied by some autofluorescence emission of the polymer.

Energy transfer from DBS to Eu^{3+} is distinctly reduced compared to the behavior in solution. The red luminescence intensity upon excitation at 267 nm is only increased by a factor of ≈2 for polyD3MA and polyTEGDMA relative to excitation at 393 nm, and decreased for BMA and BDDMA. Additionally, luminescence lifetimes are also decreased (3.3 ms in the sol, 2.2 ms in the composite). The reasons for this behavior are still not fully understood. The original assumption that the surfactant DBS undergoes hydrophobic interaction with the polyacrylate is too simple. Obviously, there is a more complex interaction between reactive groups of the acrylates (e.g. the carbonyl oxygen in the ester groups) and the particle surface, resulting in additional non-radiative relaxation processes.

In Figure 7, the admixture of the autofluorescence of polyTEGDMA excited at 366 nm and the typical red Eu^{3+} emission result in a pale white overall emission. Neat polyTEGDMA shows a blue luminescence probably due to the presence of an impurity resulting from the commercial precursors employed in this work (see SI Figure S10). While

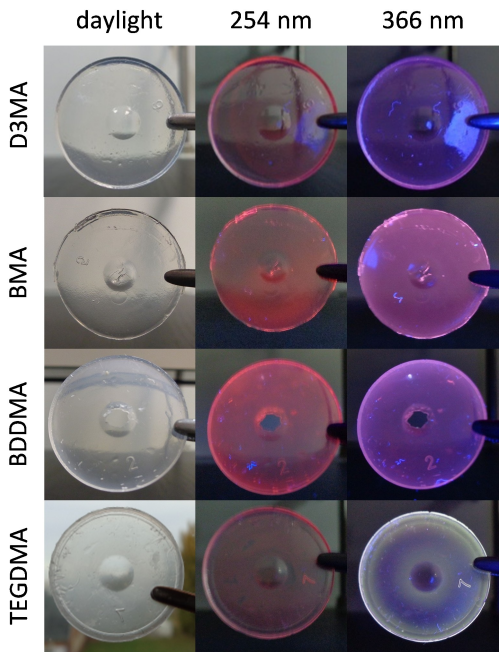

Figure 7. Organic-inorganic composites of 10% SrF_2:Eu5 and 90% polyacrylate.

these first experiments were conducted to demonstrate successfully the principle possibility of the incorporation of such hydrophobic nanoparticles into bulk polymers while retaining the luminescence properties of Eu^{3+}, we are convinced that the almost limitless flexibility of polymer chemistry will allow enhancing the brightness of such composite macroscopic materials in the nearer future.

4. Conclusion

Luminescent hydrophobic SrF_2:Eu^{3+} nanoparticles can be synthesized through fluorolytic sol-gel synthesis, followed by phase transfer extraction with SDBS into cyclohexane. The dispersion in cyclohexane is transparent and water-clear due to the small particle size. The particles have a diameter between 6 and 11 nm. The inner inorganic part of the particles consists of a nearly spherical SrF_2:Eu^{3+} core surrounded by a DBS (dodecylbenzylsulfonate) shell adsorbed at the surface.

The particles exhibit red luminescence upon excitation with UV light. Direct excitation at 393 nm shows an increase of the emission intensity with increasing Eu^{3+} content. This is direct evidence for the regular statistically distributed incorporation of Eu^{3+} into the SrF_2 matrix. Furthermore, the emission intensity increases dramatically upon excitation with short-wave UV light between 250–280 nm due to energy transfer from the aromatic moiety of the capping ligand, acting as an antenna, to Eu^{3+} centers in the outer part of the particle. Here, a comparatively low Eu^{3+} content of 5% is already enough to reach maximum brightness. These results impressively showed the dual character of DBS, acting at the same time as phase transfer agent and sensitizing ligand.

Finally, a series of transparent organic-inorganic composites with 10% inorganic mass content were prepared, embedding these nanoparticles into hydrophobic polyacrylates made from TEGDMA, BMA, BDDMA and D3MA. Transfer of the luminescence functionality into such polymers offers tremendous potential for novel hydrophobic luminescent polymer materials. Red (europium) and green (terbium) emission could directly be employed for illumination, yellow and orange colors can be achieved by mixing both ions. Additionally, viscous resins with luminescent nanoparticles offer the possibility for lithography followed by polymerization. Doping with erbium-containing nanoparticles would still broaden the scope to materials capable of amplifying modulated IR radiation (1500 nm) used for fast information transfer in optical fibers.

Experimental

Synthesis

Abbreviations. The nomenclature SrF_2:Ln*X* is used for a nominal composition $Sr_{1-x}Ln_xF_{2+x}$ with $x = X/100$ and Ln = Eu, Y. Thus, SrF_2:Eu10 is nominal $Sr_{0.9}Eu_{0.1}F_{2.1}$, SrF_2:Y5 is $Sr_{0.95}Y_{0.05}F_{2.05}$ and so on; for exact compositions, see Table 5.

Table 5. Synthesis overview.

Nr	Abbr	Nominal formula	Additive
1	SrF_2	$SrF_{1.95}(OR)_{0.05}$	0.15 eq HNO_3
2	SrF_2:Eu1	$Sr_{0.99}Eu_{0.01}F_{1.96}(OR)_{0.05}$	0.12 eq HNO_3
3	SrF_2:Eu5	$Sr_{0.95}Eu_{0.05}F_{2.00}(OR)_{0.05}$	–
4	SrF_2:Eu10	$Sr_{0.90}Eu_{0.10}F_{2.05}(OR)_{0.05}$	–
5	SrF_2:Eu20	$Sr_{0.80}Eu_{0.20}F_{2.15}(OR)_{0.05}$	–
6	SrF_2:Y5	$Sr_{0.95}Y_{0.05}F_{2.00}(OR)_{0.05}$	–

a – 0.4 M sol in ethylene glycol after synthesis; b – 0.4 M sol in cyclohexane after extraction; c – Dry powder from b; OR may be NO_3 for a or RSO_3 (DBS anion) for b.

Reactants. $Sr(OH)_2 \cdot 8H_2O$ (99%), Y_2O_3 (99.5%) and SDBS (technical) were obtained from Sigma Aldrich. Nitric acid (65%), ethylene glycol (99%) and cyclohexane (99.5%) were obtained from Carl Roth. Eu_2O_3 (99.995%) was obtained from REEtec. 72% aqueous HF was obtained from Steinebach. The exact HF concentration was determined by titration with 1 M NaOH using phenolphthalein as indicator.

$Eu(NO_3)_3 \cdot 6H_2O$ and $Y(NO_3)_3 \cdot 6H_2O$ were synthesized by dissolution of the corresponding metal oxide in a stoichiometric amount of 20% HNO_3 at ca. 60 °C, followed by evaporation of the water at ambient air below 40 °C. Drying at higher temperatures leads to undefined hydrates with less than 6 eq of crystal water.[25]

Sol in ethylene glycol (a). The synthesis is described for 100 ml sol of SrF_2:Eu10, $c = 0.4$ M. All other syntheses were performed accordingly. The amount of HF is 0.05 eq less than stoichiometrically necessary for complete fluorination. In case of very low rare-earth content, a small amount of HNO_3 is added to the Sr solution, see Table 5 for details.

9.57 g $Sr(OH)_2 \cdot 8H_2O$ (36.0 mmol) were dissolved in 50 ml of ethylene glycol. 1.78 g of $Eu(NO_3)_3 \cdot 6H_2O$ (4.0 mmol) were dissolved in 40 ml of ethylene glycol. Both solutions were mixed, followed by immediate addition of 2.09 ml (82.0 mmol = 2.05 eq) of 39.24 M aqueous HF under vigorous stirring. After stirring overnight, a nearly transparent sol was obtained. The total reaction volume was adjusted to 100 ml, resulting in an overall metal concentration of 0.4 mol L^{-1}.

Caution: HF is a hazardous agent and has to be used under restricted conditions only!

Sol in cyclohexane (b). 697 mg SDBS ($C_{18}H_{29}SO_3Na$, 2.0 mmol = 0.1 eq) were added to 50 ml of 0.4 M SrF_2:Eu10 sol in ethylene glycol and stirred for 1 h. Thereafter, 50 ml of cyclohexane were added, forming a white slurry. The slurry was stirred overnight and then allowed to settle for one day. After this time, the phases were separated. The upper phase (cyclohexane) containing the nanoparticles can be separated by decantation or with a separatory funnel. When all particles are extracted into the cyclohexane phase, the overall metal concentration is 0.4 mol L^{-1}.

Solid state NMR data. ^1H-^{13}C CP MAS NMR (100 MHz, rot 10 kHz, p15 = 1 ms). **SDBS**: 14.4, 23.1, 30.2, 32.5, 37.7, 46.6 (aliphatic $C_{12}H_{15}$), 127.2 (aromatic *C*H), 142.5 (aromatic *C*SO_3), 148.0 (aromatic *C*–$C_{12}H_{25}$). **SrF_2:Y5**: same signals plus 63.2 ppm (CH_2O of ethylene glycol).

Composites. 1 ml of acrylate monomer was mixed with 2 ml of 0.4 M sol **3 b** SrF_2:Eu5 in cyclohexane. The solvent was removed in a vacuum, resulting in a 10% dispersion of the particles in the acrylate. After addition of 10 mg diphenyl(2,4,6-trimethylbenzoyl) phosphine oxide, the dispersion was polymerized under UV excitation. In the case of MMA composites, a sol equivalent to **3 b** in cyclopentane was used for the experiments.

Methods

DLS. Dynamic light scattering was measured on a Zetasizer Nano using a 630 nm light source in quartz cuvettes. For each sample, 5 runs were averaged, 5 scans á 10 s were performed per run.

TEM. 0.4 M SrF_2:Eu^{3+} sol in cyclohexane was diluted 1:100. Some droplets were deposited on a TEM grid (carbon mesh 300, CF300-CU), dried at ambient air and placed in the sample holder (Philips CM200). The acceleration voltage was 200 kV. The tungsten filament was heated to the maximum. The software ImageJ was used for statistical TEM image analysis by manually measuring the diameter of at least 50 particles.

XRD. X-ray diffractograms of powders were obtained with a D8 ADVANCE (Bruker AXS, Karlsruhe, Bragg-Brentano geometry, LYNXEYE XE-T detector) using Cu K_α (1.542 Å) radiation and a 2ϑ step width of 0.007°. The size of the coherent scattering region L was estimated using Scherrer's equation $L = K\lambda/(\beta_{khl}\cos\vartheta)$ (with $K = 0.95$) from the 3 most intense reflections. β_{khl} is the fwhm(2ϑ) after Rachinger's correction (β_{meas}) and correction by the instrument function $\beta_0 = (9.22 \cdot 10^{-7}\vartheta^2 + 3.09 \cdot 10^{-4}\vartheta + 3.28 \cdot 10^{-2})°$: $\beta_{hkl}^2 = \beta_{meas}^2 - \beta_0^2$.

Elemental analysis and ignition loss. CHNS analysis was performed on a standard EuroVector EuroEA 3000 analyzer. The molar ratio DBS/metal was set equal to the molar ratio of sulfur and the residuum of the measured ignition loss. The calculated hypothetical ignition loss from DBS ($C_{18}H_{29}SO_3^-$) only was calculated from this ratio.

Ignition loss was determined by annealing ≈300 mg of the powder in a Pt crucible at 500 °C for 1 h in a Carbolite 4000 oven (heating rate 5 K/min).

Solid-state NMR. ^1H-^{13}C CP MAS NMR spectra were recorded with a Bruker Avance 400 spectrometer in 4 mm ZrO_2 rotors ($\nu_{rot} = 10$ kHz). Larmor frequencies of ^1H and ^{13}C were 400.1 and 100.6 MHz, respectively. 2500 scans were accumulated with a recycle delay time of 5 s and a CP contact time of 1 ms.

Absorption spectra, luminescence spectra and photoluminescence quantum yields Absorption spectra were obtained on a Specord 210 Plus from Analytik Jena in 10 and 50 mm quartz cells. Luminescence spectra as well as lifetimes were recorded with a FluoroMax-4P from Horiba Jobin Yvon in 10 mm quartz cells. Photoluminescence quantum yields Φ_{PL} were determined relative to standard organic dyes (Coumarin 102 in ethanol, $\Phi_{PL} = 0.76$; terphenyl in cyclohexane $\Phi_{PL} = 0.93$).[26] Briefly, absorption spectra of the reference dyes and samples were recorded in 10 mm or 50 mm quartz cuvettes and diluted, if needed, to obtain an absorbance lower than 0.1 at 393 nm or 267 nm for excitation of Eu^{3+} or DBS anion, respectively. The emission of the same solutions was measured at the respective excitation wavelength. The photoluminescence quantum yield Φ_{PL} is calculated by multiplication of the known Φ_{PL} of the reference dyes with the ratio of the absorption corrected emission of the sample and the reference dye, taking also into account the refractive indices of the solvents. The exact description of the mathematical calculations can be found elsewhere.[27] The uncertainty of measurement amounted to ±10%. Luminescence lifetimes were recorded using the TCSPC accessory in single photon counting mode with a collection time up to 175 ms. Lifetime profiles were fitted using a biexponential decay $I(t) = A_1 e^{-t/\tau_1} + A_2 e^{-t/\tau_2} + C$. Mean lifetimes were calculated according to $\bar{\tau} = (A_1\tau_1 + A_2\tau_2)/(A_1 + A_2)$.[18]

Acknowledgements

Gudrun Scholz is gratefully acknowledged for measuring and discussing solid-state NMR spectra, Stefan Mahn for recording TEM images and Dominik Al-Sabbagh for X-ray diffraction.

Conflict of Interest

The authors declare no conflict of interest.

Keywords: Nanoparticles · Fluorides · Sol-gel process · Organic-inorganic hybrid composites

[1] a) S. Gai, C. Li, P. Yang, J. Lin, *Chem. Rev.* **2014**, *114*, 2343–2389; b) J. Zhou, Q. Liu, W. Feng, Y. Sun, F. Li, *Chem. Rev.* **2015**, *115*, 395–465.
[2] a) F. Wang, X. Liu, *Chem. Soc. Rev.* **2009**, *38*, 976–989; b) M. Haase, H. Schäfer, *Angew. Chem. Int. Ed.* **2011**, *50*, 5808–5829; *Angew. Chem.* **2011**, *123*, 5928–5950.
[3] a) B. Ritter, P. Haida, F. Fink, T. Krahl, K. Gawlitza, K. Rurack, G. Scholz, E. Kemnitz, *Dalton Trans.* **2017**, *46*, 2925–2936; b) B. Ritter, P. Haida, T. Krahl, G. Scholz, E. Kemnitz, *J. Mater. Chem. C* **2017**, *5*, 5444–5450.
[4] I. Richman, *J. Chem. Phys.* **1964**, *41*, 2836–2837.
[5] B. P. Sobolev, K. B. Seiranian, L. S. Garashina, P. P. Fedorov, *J. Solid State Chem.* **1979**, *28*, 51–58.
[6] a) A. K. Cheetham, B. E. F. Fender, M. J. Cooper, *J. Phys. C* **1971**, *4*, 3107–3121; b) J. P. Laval, A. Mikou, B. Frit, G. Roult, *Solid State Ionics* **1988**, *28–30, Part 2*, 1300–1304; c) T. Krahl, G. Scholz, E. Kemnitz, *J. Phys. Chem. C* **2014**, *118*, 21066–21074.
[7] a) B. Ritter, T. Krahl, G. Scholz, E. Kemnitz, *J. Phys. Chem. C* **2016**, *120*, 8992–8999; b) A. Antuzevics, M. Kemere, G. Krieke, *J. Alloys Compd.* **2018**, *762*, 500–507.
[8] a) E. Kemnitz, U. Groß, S. Rüdiger, C. S. Shekar, *Angew. Chem. Int. Ed.* **2003**, *42*, 4251–4254; *Angew. Chem.* **2003**, *115*, 4383–4386; b) S. Rüdiger, E. Kemnitz, *Dalton Trans.* **2008**, 1117–1127; c) E. Kemnitz, J. Noack, *Dalton Trans.* **2015**, *44*, 19411–19431.
[9] a) F. Wang, X. Fan, D. Pi, M. Wang, *Solid State Commun.* **2005**, *133*, 775–779; b) P. Ptacek, H. Schäfer, K. Kömpe, M. Haase, *Adv. Funct. Mater.* **2007**, *17*, 3843–3848; c) R. E. Muenchausen, L. G. Jacobsohn, B. L. Bennett, E. A. McKigney, J. F. Smith, J. A. Valdez, D. W. Cooke, *J. Lumin.* **2007**, *126*, 838–842; d) C. R. Ronda, in *Luminescence*, Wiley VCH, Weinheim, **2007**, pp. 1–34; e) A. Jain, P. G. J. Fournier, V. Mendoza-Lavaniegos, P. Sengar, F. M. Guerra-Olvera, E. Iñiguez, T. G. Kretzschmar, G. A. Hirata, P. Juárez, *J. Nanobiotechnol.* **2018**, *16*, 26.
[10] S. Mahn, E. Kemnitz, *J. Appl. Polym. Sci.* **2019**, *136*.
[11] a) J. Noack, C. Fritz, C. Flugel, F. Hemmann, H.-J. Glasel, O. Kahle, C. Dreyer, M. Bauer, E. Kemnitz, *Dalton Trans.* **2013**, *42*, 5706–5710; b) J. Noack, L. Schmidt, H.-J. Glasel, M. Bauer, E. Kemnitz, *Nanoscale* **2011**, *3*, 4774–4779.
[12] L. Schmidt, S. Mahn, E. Kemnitz, *RSC Adv.* **2017**, *7*, 56266–56270.
[13] D. D. Wagman, W. H. Evans, V. B. Parker, R. H. Schumm, I. Halow, S. M. Bailey, K. L. Churney, R. L. Nuttall, *J. Phys. Chem. Ref. Data* **1982**, *11*, Suppl. 2.
[14] G. R. Fulmer, A. J. M. Miller, N. H. Sherden, H. E. Gottlieb, A. Nudelman, B. M. Stoltz, J. E. Bercaw, K. I. Goldberg, *Organometallics* **2010**, *29*, 2176–2179.
[15] B. Ritter, T. Krahl, K. Rurack, E. Kemnitz, *J. Mater. Chem. C* **2014**, *2*, 8607–8613.
[16] R. J. Wiglusz, T. Grzyb, A. Bednarkiewicz, S. Lis, W. Strek, *Eur. J. Inorg. Chem.* **2012**, *2012*, 3418–3426.
[17] a) C. Lorbeer, J. Cybinska, E. Zych, A. V. Mudring, *Opt. Mater.* **2011**, *34*, 336–340; b) P. Cortelletti, M. Pedroni, F. Boschi, S. Pin, P. Ghigna, P. Canton, F. Vetrone, A. Speghini, *Cryst. Growth Des.* **2018**, *18*, 686–694.
[18] a) A. Podhorodecki, M. Banski, J. Misiewicz, M. Afzaal, P. O'Brien, D. Cha, X. Wang, *J. Mater. Chem.* **2012**, *22*, 5356–5361; b) C. Caron, D. Boudreau, A. M. Ritcey, *J. Mater. Chem. C* **2015**, *3*, 9955–9963.
[19] a) X. Liu, S. Tao, N. Deng, Y. Liu, B. Meng, B. Xue, G. Liu, *Anal. Chim. Acta* **2006**, *572*, 134–139; b) G. Shao, R. Kautz, S. Peng, G. Cui, R. W. Giese, *J. Chromatogr. A* **2007**, *1138*, 305–308.
[20] S. Nigam, V. Sudarsan, R. K. Vatsa, *Eur. J. Inorg. Chem.* **2013**, *2013*, 357–363.
[21] a) J. Shen, L.-D. Sun, J.-D. Zhu, L.-H. Wei, H.-F. Sun, C.-H. Yan, *Adv. Funct. Mater.* **2010**, *20*, 3708–3714; b) J. P. Zuniga, S. K. Gupta, M. Abdou, Y. Mao, *ACS Omega* **2018**, *3*, 7757–7770.
[22] A. K. Parchur, R. S. Ningthoujam, S. B. Rai, G. S. Okram, R. A. Singh, M. Tyagi, S. C. Gadkari, R. Tewari, R. K. Vatsa, *Dalton Trans.* **2011**, *40*, 7595–7601.
[23] G. Mialon, M. Gohin, T. Gacoin, J.-P. Boilot, *ACS Nano* **2008**, *2*, 2505–2512.
[24] C. Hansch, A. Leo, D. Hoekman, *Exploring QSAR/2, Hydrophobic, electronic, and steric constants*, American Chemical Society, Washington, DC, **1995**.
[25] S. Siekierski, T. Mioduski, M. Salomon, in *Scandium, Yttrium, Lanthanum and Lanthanide Nitrates, Vol. 13*, Pergamon Press, **1983**.
[26] a) R. E. Kellogg, R. G. Bennett, *J. Chem. Phys.* **1964**, *41*, 3042–3045; b) D. Giaume, V. Buissette, K. Lahlil, T. Gacoin, J. P. Boilot, D. Casanova, E. Beaurepaire, M. P. Sauviat, A. Alexandrou, *Prog. Solid State Chem.* **2005**, *33*, 99–106; c) B. Mutelet, P. Perriat, G. Ledoux, D. Amans, F. Lux, O. Tillement, C. Billotey, M. Janier, C. Villiers, R. Bazzi, S. Roux, G. Lu, Q. Gong, M. Martini, *J. Appl. Phys.* **2011**, *110*, 094317.
[27] a) K. Rurack, in *Standardization and Quality Assurance in Fluorescence Measurements I: Techniques* (Ed.: U. Resch-Genger), Springer Berlin Heidelberg, Berlin, Heidelberg, **2008**, pp. 101–145; b) K. Rurack, M. Spieles, *Anal. Chem.* **2011**, *83*, 1232–1242.

Manuscript received: January 27, 2020
Revised manuscript received: March 31, 2020
Accepted manuscript online: April 8, 2020
Version of record online: May 28, 2020